Title
Contrasting Impacts of the South Pacific Split Jet and the Southern Annular Mode Modulation on Southern Ocean Circulation and Biogeochemistry

Journal
Paleoceanography and Paleoclimatology, 33(1)

ISSN
2572-4517

Authors
Chiang, John CH
Tokos, KS
Lee, S-Y
et al.

Publication Date
2018

DOI
10.1002/2017pa003229

Peer reviewed

Contrasting impacts of the South Pacific Split Jet and the Southern Annular Mode modulation on Southern Ocean circulation and biogeochemistry

John C. H. Chiang[1], K. S. Tokos[2], S.-Y. Lee[3], and K. Matsumoto[2]

[1] Dept. of Geography and Berkeley Atmospheric Sciences Center, University of California, Berkeley CA 94720-4740

[2] Dept. of Earth Sciences, University of Minnesota, Minneapolis MN 55455

[3] Research Center for Environmental Changes, Academia Sinica, Taipei, Taiwan

Corresponding author: John Chiang (jch_chiang@berkeley.edu)

Key Points:

- Ocean changes associated with wintertime South Pacific Split Jet is contrasted against those associated with Southern Annular Mode
- Pronounced but different changes are seen to the South Pacific subtropical gyre, Drake Passage throughflow, and SAMW/AAIW formation
- Changes to ventilation of deep waters occur, but impact on atmospheric CO_2 is limited by compensating effects of biology and solubility

Abstract

A recent hypothesis postulated that paleoclimate changes to the Southern Hemisphere westerlies were characterized by the modulation of the wintertime South Pacific Split Jet. We explore this hypothesis further through simulating changes to the ocean circulation from Split Jet modulation, contrasting them against changes associated with the wintertime Southern Annular Mode (SAM). Three responses distinguish the Split Jet from the SAM impact on ocean circulation. (i) A weaker Split Jet strengthens the South Pacific subtropical gyre, leading to stronger western boundary currents and warming of the SSTs surrounding New Zealand. (ii) A positive SAM leads to an increase in the Antarctic Circumpolar current and specifically Drake Passage throughflow; and (iii) A weaker Split Jet leads to increased formation of Subantartic Mode Water whereas a positive SAM leads to increased Antarctic Intermediate Water. Both a weaker Split Jet and positive SAM lead to increased Southern Ocean meridional overturning circulation, though it is more pronounced for the latter. However, enhanced ventilation of deep water in both cases increases atmospheric pCO_2 by only 1-3 ppm, because the associated cooling and efficient nutrient utilization in the model effectively negates the venting of deep ocean carbon. Both a weaker Split Jet and positive SAM enhance oxygenation of the deep ocean and intermediate waters but diminish oxygenation of the eastern equatorial Pacific. Our results provide guidance to distinguish SAM-like changes from Split Jet-like changes in paleoceanographic records, and we discuss the case of early deglacial transition to Heinrich 1.

Index terms: 1635 Oceans, 4901 Abrupt/rapid climate change, 4912 Biogeochemical cycles, processes, and modeling, 4223 Descriptive and regional oceanography, 4576 Western boundary currents

1. Introduction

Changes to the southern hemisphere westerlies and their resulting impact on the ocean circulation feature prominently in current conceptualization and debates on paleoclimate changes. The pioneering studies are attributed to Toggweiler [*Toggweiler and Samuels*, 1998], who showed that in the limit of no vertical mixing, a large-scale ocean overturning circulation could be maintained by a wind-driven Antarctic circumpolar current. The wind-driven upwelling brings up waters from the deep at the latitudes of the Drake Passage, and in so doing ventilate the deep ocean. This ventilation brings CO_2-rich deep ocean waters to the surface and exerts strong control on atmospheric CO2.

Virtually all studies linking southern hemisphere westerlies to ocean circulation and paleoclimate change assume (implicitly or explicitly) a zonally symmetric change to the westerlies, usually a meridional shift (e.g. *Toggweiler* 2009) but also increase in the intensity or variation in its meridional width (e.g. *Moreno et al.*, 2010). This conceptual model follows the Southern Annular Mode (SAM) variation in the westerlies that dominates current literature in dynamical meteorology and climate (e.g. *Cai et al.*, 2005; *Marshall*, 2003; *Thompson and Wallace*, 2000). However, as paleoproxies occupy a limited number of discrete locations, few studies question this assumption because of the inherent difficulty in distinguishing between zonally symmetric from other kinds of westerly wind changes (there are a few notable exceptions, including *Fletcher and Moreno* [2011] and *Bostock et al.* [2015]).

In a recent study *[Chiang et al., 2014]*, we auditioned another type of change for southern hemisphere westerly changes in paleoclimate: the modulation of the South Pacific Split Jet. Southern hemisphere westerlies are largely zonally symmetric in the austral summer, but in winter exhibit a pronounced zonal asymmetry (Figure 1a). In this season, there is a single westerly jet over the Indian sector, but then splits in to a northern subtropical and a southern subpolar branch at the longitudes of Australia. This split continues across the South Pacific, until the subpolar branch weakens, and a single jet again emerges east of South America. This is the so-called Split Jet [*Bals-Elsholz et al.*, 2001; *Taljaard*, 1972].

Current dynamical explanations link the zonal asymmetry in the Southern Hemisphere wintertime westerlies to the presence of the strong summer Asian monsoon [*Nakamura and Shimpo*, 2004]. The northern-positioned convection induces a Hadley circulation with a strong southern branch, that in turn drives a strong southern subtropical jet over the Australia/South Pacific sector through the meridional advection of angular momentum by the upper branch of the cell (Figure 1a). This strong subtropical jet acts as waveguide, such that atmospheric transient eddies from the Indian Ocean sector entering the South Pacific preferentially get swept into this jet [*Nakamura and Shimpo*, 2004]. Otherwise, these transient eddies would continue to propagate zonally over the South Pacific midlatitudes, resulting in strengthened midlatitude westerlies through wave-mean flow interactions. In general, the zonal asymmetry in the southern hemisphere storm track has been attributed to the zonal asymmetry in the tropical SST and its resulting effect on tropical convection and planetary wave propagation [*Inatsu and Hoskins*, 2004].

Our hypothesis, as stated in Chiang et al. (2014), is that paleoclimate changes to the southern hemisphere westerlies are characterized by a modulation of this Split Jet. Specifically, during the cold North Atlantic stadial periods, the Split Jet weakens and the southern hemisphere wintertime westerlies more closely resemble a single zonally-symmetric jet. This contrasts with current notions that southern hemisphere westerlies shifted southward (i.e. a more positive SAM) during North Atlantic stadials [e.g. *Toggweiler*, 2009]. The reason for a weaker Split Jet is that

North Atlantic stadials are associated with a weakening of the Northern hemisphere summer monsoons and a southward shift of the ITCZ (e.g. *Chiang and Friedman*, 2012, and references therein). The South Pacific subtropical jet thus weakens, and by the dynamical arguments above this ultimately leads to a weakening of the Split Jet. [*Chiang et al.*, 2014] lent support to the hypothesis by noting that land-based proxy records of abrupt changes over New Zealand and Patagonia appear to be consistent with a modulation of the Split Jet. *Bostock et al.* [2015] also proposed a modulation of the Split Jet as a potential explanation for changes to the latitude of the subtropical front south of New Zealand.

The most intriguing implication of the hypothesis is the change to the wind stress over the ocean and potential ramifications for ocean circulation; this is the focus of this paper. As shown in *Chiang et al. [2014]*, a weaker Split Jet leads to a change in the wind stress curl over the South Pacific, specifically a marked southward shift in the zero wind stress curl line from the subtropical latitudes towards the southern tip of South America (see Figure 5 of *Chiang et al.* 2014, and also Figure 2b). This is a remarkable change to the wind stress pattern, with strong implications for the wind-driven ocean circulation in the South Pacific and in particular the subtropical gyre.

The goal of this study is to explore the consequences of a weakened Split Jet to the Southern Ocean circulation and biogeochemistry, specifically carbon and oxygen. We undertake ocean model simulations to explore the ocean circulation response to the specified westerly changes imposed on the model ocean. We contrast the simulated changes to those induced by a wintertime modulation of the SAM, to contrast the impacts of the two competing hypotheses for Southern Hemisphere westerlies on ocean circulation. We will then compare the changes to ocean paleoproxy records to assess how each are consistent (or not) to records of Southern

Ocean response the early deglacial period, specifically climate changes associated with the transition to Heinrich 1.

2. Materials and Methods

2.1 Model

We undertake ocean-only simulations with the Parallel Ocean Model version 2 that comes as part of the Community Earth System Model (CESM) 1.2.2 [*Danabasoglu et al.*, 2011]. The component set used is a scientifically validated and supported compset of CESM "2000_DATM%NYF_SLND_CICE_POP2_DROF%NYF_SGLC_SWAV". It includes prognostic ocean (POP2) and sea ice (CICE) modules, but with a prescribed 'data' atmosphere (DATM) and 'data' runoff (DROF). We use the standard gx1v6 'displaced pole' grid. The CESM has been used extensively, including studies examining the ocean response to southern hemisphere westerlies (e.g. *Gent and Danabasoglu*, 2011)

We include a simple biogeochemistry (BGC) module developed specifically for POP2 and made available to us by Keith Lindsay at NCAR. The BGC module follows the "BIOTIC" formulation of OCMIP and features the so-called "nutrient-restoring" or diagnostic export production [*Najjar et al.*, 2007]. Essentially, phosphate concentration in the surface ocean of the model is nudged toward, or restored to, observed phosphate climatology on a time scale of biological production of 30 days. For example, in upwelling regions, where phosphate supply is large, the nudging and thus the diagnosed export production are large. Export production is partitioned into particulate and dissolved phases. State variables in this BGC module include phosphorus (PO_4, DOP, POP), carbon (DIC, DOC, POC), oxygen, and alkalinity. The stoichiometry that relates the elements in organic matter is fixed: $P{:}C{:}O_2=1{:}117{:}-170$. Biological production of organic matter near the surface removes these elements in exactly these ratios.

Respiration of organic matter in the ocean interior releases these elements in the same ratios. Wind-driven gas exchange formulation allows CO_2 and O_2 to be exchanged between the atmosphere and surface ocean. Atmospheric pCO_2 is thus a prognostic variable; it is 284.7 ppm in the equilibrium state. Atmospheric O_2 is fixed at the modern mixing ratio. The OCMIP formulation continues to respire organic matter even after O_2 runs out, assuming that nitrate, which is not a model variable, would serve as the electron acceptor in respiration. This BGC module has been thoroughly examined in the intercomparison project OCMIP Phase 2 [Najjar et al., 2007]. It is appropriate for this study, because export production and associated net air-sea CO_2 flux would respond to changes in wind-induced upwelling.

2.2 Forcing Data

The data atmosphere of CESM uses the ‘Co-ordinated ocean-ice reference experiments’ version 2 (CORE v2) normal year forcing [*Large and Yeager*, 2009] for driving the ocean model. They are 6-hourly fields derived from several observational/reanalysis datasets, and intended as a common ocean driver to compare different ocean model simulations. In addition to the ‘normal year’ forcing, CORE v2 also includes forcings for individual years from 1948 through 2009. For our purposes, we restrict ourselves to forcing data from 1979 onwards to avoid a potential discontinuity resulting from the assimilation of satellite data starting in 1979.

To apply perpetual weak or strong Split Jet scenarios, we first derive surface spatial patterns associated with Split Jet variation. We derive an interannual index of the Split Jet from 1979-2015 (see section 3), then use it to obtain a spatial pattern of the forcing field every 6-hours. Using the zonal wind stress (taux) for 00H of June 1 as an example, first a 21-day average of taux centered on 00H is formed (so taking all 00H time points 10 days before and 10 days after, and averaging), for each individual year in the CORE v2 taux fields. The 21-day average is applied to remove weather noise and obtain a reasonable estimate of the climate state around that time. We then regress the normalized interannual Split Jet index against each gridpoint of taux for 00H over 1979-2009 (the CORE v2 interannual data is only available until 2009) to obtain a spatial field corresponding to the change in the taux for 1 standard deviation change in the Split Jet index. This spatial pattern is then multiplied by 2 and then added to the CORE v2 normal year taux to form a representative strong Split Jet taux field for 00H on June 1; to get the weak Split Jet field, we multiply by -2 and then add to the CORE v2 normal year; the magnitude of our forcing anomalies is thus set to ±2 standard deviations of the interannual variability. Our study differs from many others investigating the ocean circulation changes to southern hemisphere westerly changes in that the wind perturbations we apply- while large - are spatially realistic and physically realizable.

Since the Split Jet and its variability only occur in the austral winter, we produce these forcing fields every 6-hours from 00H of June 1 through 18H of September 30 only. This is repeated for each forcing field in the CORE v2, including: zonal and meridional surface wind stress, zonal and meridional winds at 10m, air density, temperature and specific humidity at 10m, and sea level pressure. These fields are then used to drive the POP2 model for the strong and weak Split Jet cases. The same is also done to the shortwave and longwave radiative forcing in CORE v2, but they are at daily resolution; for those, we apply the same procedure but to daily fields. Finally, the precipitation forcing in CORE v2 only has monthly fields, so we do the regression for each month from June through September.

For forcings associated with opposite phases (positive and negative) of the SAM, we follow the same procedure as for the Split Jet but using an interannual index for the annular mode-like variation; section 3 describes how the SAM index is obtained.

2.3 Experiments

We first ran the POP under the standard CORE v2 normal year forcing for 500 years to obtain a reasonable starting point. We then branch off the simulation into two runs, one with perpetual weak Split Jet conditions and the other with perpetual strong Split Jet forcing. We run these two cases for 600 years each so that the wind-driven surface circulation can come into quasi-equilibrium, and changes to the deep ocean circulation are captured; examination of the timeseries of southern ocean meridional overturning circulation strength and Drake Passage throughflow indicate that this is the case (not shown). Our assessment of the impact of the Split Jet modulation on ocean circulation and biogeochemistry is done by comparing the difference in the annual mean climatology over the last 20 years of each simulation. Prior to analysis, the ocean model output was regridded from its native gx1v6 horizontal resolution to a uniform 1°x1° grid. Mean fields reported here (in figures 5,6, and 7) are taken as the average of the weak Split Jet and strong Split Jet annual mean climatologies. Finally, we undertake an analogous set of two runs for the positive and negative SAM cases.

3. Interannual variability of the Southern Hemisphere wintertime westerlies

We apply an Empirical Orthogonal Function (EOF) analysis on the June-September averaged zonal wind anomalies from 1979-2015 using the NCEP reanalysis to extract the dominant interannual variability for the austral winter westerlies. Since the expression of the Split Jet is most pronounced in the upper troposphere, we use the 3-dimensional zonal winds in the calculation; this contrasts with the standard derivation of the SAM that uses the first EOF of sea level pressure over the southern extratropics. The latitude range was restricted to 15°S-80°S, and the vertical co-ordinate was interpolated in 100mb intervals from 150mb to 950mb. Prior to the calculation, the anomaly data was multiplied by the square root of the cosine of latitude to weight for area.

The first 3 modes are significant (using the 'Rule N' test [*Preisendorfer*, 1988]) and well separated from each other (applying North's Rule of Thumb [*North et al.*, 1982]). The first mode, accounting for 22.2% of the variance, has the distinct signature of the modulation of the Split Jet: the primary signature is a positive loading of winds over the midlatitude South Pacific (35-55°S), and negative loading to the north and south of this feature (Figure 1b): this indicates a weakening of the Split Jet with weaker subtropical and subpolar jets, and stronger midlatitude jet. The second mode, accounting for 16.1% of the variance, has a more zonally-symmetric structure with negative loadings in the subtropical latitudes (25-45°S) and positive loadings from 45-70°S (Figure 1c). The mode represents a poleward shift of the midlatitude jet, resembling an annular-mode like modulation. In fact, the 2nd principal component (PC2) correlates with a standard index for the SAM [*Mo*, 2000] averaged over June-Sep at $r = 0.88$, significant at the 0.1% level; thus, PC2 is essentially the SAM index for the austral winter, and we will refer to mode 2 as the SAM mode from now on. On the other hand, PC1 and 3 are not significantly correlated with the SAM index. The third mode, accounting for 10.3% of the variance, is a teleconnection pattern spanning from the Maritime continent across Australia to the high latitude South Pacific.

Our EOF results indicate that we have successfully extracted the Split Jet (mode 1) from SAM (mode 2) variations from data, and that they are linearly independent. We use these two modes to derive anomalous forcing fields for each influence, through regression on the corresponding normalized PC onto the CORE v2 interannual fields (see section 2).

4. Ocean circulation changes

We focus on key features of the Southern Ocean circulation that exhibit different responses between the Split Jet and SAM wind forcings. For the surface circulation, they include the South Pacific subtropical gyre circulation and the Antarctic Circumpolar current (ACC). For the deep circulation, they include the meridional overturning circulation and deep ocean ventilation, and formation of intermediate waters. Recall that the simulated ocean fields we use are the last 20 years of 600-year simulations, and with the same atmospheric forcing applied each year; hence, the ocean circulation changes reported in this section (and section 5) can be thought of as equilibrated ocean changes in response to permanent Split Jet or SAM changes.

4.1 <u>Surface ocean circulation</u>

4.1.1 Subtropical gyre and currents off Eastern Australia and New Zealand

Split Jet response: As shown in Chiang et al. [2014], one of the most striking features of a weak Split Jet, contrasted with a strong Split Jet, is a change in the sign of the wind stress curl over the subtropical South Pacific (30°S-40°S) to positive values, resulting in a southward shift of the subtropical zero wind-stress curl line in the South Pacific (Figures 2a and 2b). This induces a northward Sverdrup interior flow in the subtropical South Pacific that must be compensated for by a stronger western boundary current, implying a strengthened and southward shifted oceanic subtropical gyre. This feature is seen in the simulated ocean circulation changes, most noticeably by the change to the barotropic streamfunction that shows a stronger and more southward South Pacific subtropical gyre circulation for the weak Split Jet (Figure 3b). With this, the southward extent of the South Pacific subtropical gyre resembles that for the South Indian in the mean (Figure 3a).

Predictions of a stronger and more poleward-penetrating western boundary current is indeed seen for the East Australian Current (figure 4b). The East Australian Current splits from the Australian continental shelf at the latitude of the northern tip of New Zealand, though some of the current proceeds farther south (see figure 4a for a schematic of the various currents). The flow then moves eastwards to the northern tip of New Zealand as the Tasman Front, then turns due south at the northern edge of North Island to form the East Auckland current, and then along the eastern coast of North Island as the East Cape Current; these are the continuations of the western boundary current. This boundary current finally splits away from New Zealand into the southeastern Pacific by the latitude of Chatham Rise. In the weak Split Jet, these flows are significantly strengthened (figure 4b). Farther south, the Antarctic Circumpolar Current south of Tasmania and New Zealand is also strengthened, but this anomalous flow heads northwards along the eastern coast of South Island and veers eastwards at the latitude of Chatham Rise to merge with the current originating from the north.

A consequence of the stronger and more poleward-penetrating subtropical gyre is warmer sea surface temperatures off the eastern coasts of Australia and New Zealand (Figure 4b), by up to 2°C for the difference between the weak and strong Split Jet cases. This is notable as New Zealand glaciers are known to have rapidly retreated during the Younger Dryas, indicating warmer conditions; this is consistent with the Chiang et al. [2014] hypothesis of a weaker Split Jet during that time. A stronger subtropical gyre also leads to a stronger equatorward return flow over the eastern South Pacific, leading to moderately cooler SSTs there (Figure 4b).

Finally, there are intriguing though smaller northward shifts to the southern extent of the subtropical gyre over the South Indian and South Atlantic oceans, as indicated by the changes to the barotropic streamfunction (Figure 3b). The most notable consequence of this is a strong cooling in the South Atlantic around 42°S at the poleward end of the South Atlantic subtropical gyre boundary, near the South American coastline (figure 4b).

SAM response: The response of the ocean circulation to variation in the SAM produces little change to the strength of the subtropical gyre circulation but does affect the East Australian boundary current. The positive SAM (southward-shifted westerlies) relative to the negative SAM leads to a more southward extension of the East Australian Current (Figure 4c). The poleward extension is consistent with the increased positive wind stress in the interior South Pacific between 40-50°S (Figure 2c, d). By Sverdrup balance, the latter implies increased interior northward flow at those latitudes. A consequence of this is a reduced eastward current by the Tasman Front where the East Australian Current partly separates from the coast around 35°S, but a stronger eastward current around 50°S where the East Australian Current merges with the ACC (figure 4c). As a result, surface temperatures warm over the southeastern coast of Australia and the Tasman sea, though not as pronounced as for the weaker Split Jet case (Figure 4b). By contrast, the SSTs east of the North Island of New Zealand cools, presumably because of the reduced East Auckland and East Cape Currents; this is opposite to that seen for the weaker Split Jet. This pattern of SST changes surrounding New Zealand was also obtained in an ocean model study by *Cai et al.* [2005] to positive SAM winds.

4.1.2 Antarctic Circumpolar Current and Drake Passage throughflow

Split Jet response: There is a modest increase to ACC and Drake Passage throughflow for a weaker Split Jet relative to a strong Split Jet, as indicated by the barotropic streamfunction anomaly (figure 3b) that shows increased meridional gradient in streamfunction values across the ACC latitudes. Drake Passage throughflow (evaluated at 69.5°W) is 116Sv in the strong Split Jet case whereas in the weak Split Jet case is 133Sv, an increase of 17Sv.

SAM response: On the other hand, the positive SAM leads to a pronounced increase in the volume transport of the Antarctic Circumpolar Current (ACC). Transport across the Drake Passage increases from 100 Sv in the negative SAM run, to 142Sv, an increase of 42Sv, mainly due to increased flow in the southern portion of the Drake Passage (figure 4c). The reason for this increase is that the positive phase of the SAM leads to increased wind stress over the Drake Passage latitudes (~60°S; see figure 1c). In the absence of a zonal pressure gradient to counter the increased wind stress, an increased form drag at the ocean floor is required to balance it, implying a stronger ACC circulation.

4.2 Overturning circulation

Split Jet response: Changes to the wind stress over the South Pacific leads to a pronounced alteration in the spatial pattern of surface upwelling and downwelling. For a weak Split Jet, the zone of upwelling shifts northwards over the South Pacific sector to around 50°S, and downwelling is increased to the north of it (Figure 5b). This has the effect of enhancing the spatial contrast of mean upwelling and downwelling over the South Pacific sector, making it resemble the spatial structure of upwelling over the other ocean basins (Figure 5a). The sense is that a weak Split Jet reduces the zonal asymmetry in the spatial pattern of surface upwelling and downwelling.

The increased downwelling north of 40°S in the South Pacific leads to increased subduction rate of Subantarctic Mode Water (SAMW) in the South Pacific. The rate increase is suggested by a decrease in the ideal age of waters in the subduction region (ideal age is an idealized tracer indicating the elapsed time since a water parcel's last exposure to the surface), centered around 800m and 30°S (Figure 6b). This increased formation of SAMW does not occur over the other basins, where downwelling does not increase. The change to the Pacific MOC

(Figure 6e) shows a slight increase to the subduction of southern subtropical surface waters into the thermocline, consistent with the increased rate of SAMW formation.

A weaker Split Jet also leads to increased rate of Antarctic Bottom Water (AABW) formation. Significantly younger ideal age values at the bottom of the South Pacific (Fig 6b) suggests an increased rate of deep water formation, and this is collaborated by changes to the Pacific MOC (Fig 6e) showing increased northward flow at the bottom of the South Pacific.

SAM response: Significant changes to the surface upwelling and downwelling also occurs, with increased upwelling south of ~55°S and increased downwelling to the north of it (Figure 5c). This occurs over all three basins; the sense is that the mean spatial pattern of upwelling and downwelling over the Southern ocean is enhanced. The increased midlatitude subduction over all basins leads to increased formation of Antarctic Intermediate Water (AAIW); this interpretation is supported by the decrease in ideal age of waters around 40°S and 1000m in depth (Figure 6c), as well as changes to the Pacific MOC (Fig 6f) showing increased subduction of surface waters around ~50°S into the AAIW depths.

A more notable consequence of a positive SAM is the increased rate of bottom water formation, significantly stronger than that for the weak Split Jet case. The increased rate of formation of Antarctic Bottom Water (AABW) is indicated by its considerably younger ideal age (Figure 6c), and the corresponding increase to the northward transport of bottom waters in the Pacific as indicaed by the Pacific MOC change (Figure 6f). This has consequences for the oceanic carbon cycle, which we elaborate on in Section 5.

5. Ocean biogeochemical changes

The response of ocean circulation to the Split Jet and SAM wind forcings has important implications for nutrient redistribution, water mass residence time, and deep water temperatures. In turn, these have significant effects on biological production and air-sea gas exchange. Here we focus on the effects of the ocean circulation changes to the biogeochemically important elements, oxygen and carbon.

5.1 Oceanic Oxygen

Dissolved oxygen (O_2) is a sensitive indicator of ocean physics and biogeochemistry. Many areas of the world surface ocean are close to O_2 saturation, because the residence time in those areas is comparable to or exceeds the typical equilibration time scale of O_2 exchange with the atmosphere. To first order, it is SST that determines the O_2 solubility and thus surface concentration. Vertical mixing transports this surface O_2 signal into the ocean interior, where respiration of organic matter consumes O_2. Where dissolved O_2 becomes too low for oxic respiration, nitrate replaces O_2 as the terminal electron acceptor in the process of denitrification. This process changes the distribution and whole ocean inventory of nitrate, which limits biological production in many parts of the world ocean. Thus, oceanic O_2 is not only an indicator of ocean physics and biogeochemistry, but a driver of the latter at the same time.

In this study, increased deep ocean ventilation in both the weak Split Jet and positive SAM simulations delivers dissolved O_2 in great abundance, as seen in the Pacific Ocean (Figure 7b,c). In the positive SAM case, the positive O_2 anomaly increases throughout the water column in Southern Ocean (Figure 7c), where meridional overturning is strong and deep (Figure 6f). Outside the Southern Ocean, the deep O_2 anomaly is large (~150 μmol/kg) and extends to the far northern extent of the Pacific basin. The same positive O_2 anomaly in the deep ocean is also seen, but is weaker overall in the weak Split Jet simulations (Figure 7b). Higher in the water column, there is a small positive O_2 anomaly associated with the SAMW waters in the weak Split Jet case and with the AAIW waters in the positive SAM case; these are consistent with the increased rate of SAMW/AAIW formation inferred from the ideal age and PMOC changes (Figure 6). Spatially, the strong positive O_2 anomaly for the weak Split Jet case is restricted to the South Pacific (Figure 8a). In contrast, the zonal symmetry of the forcing in the SAM runs clearly translates to enhanced oxygenation occurring in all sectors of the circumpolar current (Figure 8b).

Much of this positive O_2 anomaly can be understood in terms of apparent oxygen utilization (AOU), which shows nearly the same spatial pattern as O_2 along the 150 °W section, so that O_2 and AOU are tightly clustered about the 1:1 line in a scatter plot (figure not shown). In a parcel of seawater, AOU is defined as the difference between the theoretical O_2 concentration at saturation, calculated from the parcel's temperature, and the observed/simulated O_2 concentration. One assumes in AOU calculation that the parcel, when it was last at the surface, was at saturation. It follows then that a parcel of interior water with AOU of zero is "fully charged" with O_2, and a parcel with a large AOU has experienced significant O_2 depletion due to respiration. In order to explain the positive O_2 anomalies in the weak Split Jet (Figure 7b) and positive SAM (Figure 7c) simulations in terms of AOU, either the deep ventilation became more vigorous, the interior respiration became smaller, or a combination of the two.

Our analysis shows that it is largely a more vigorous deep ventilation (Figure 6), because respiration did not change much. In the OCMIP formulation, biological production largely keeps up with ocean circulation changes and associated nutrient redistribution, so that global carbon export in weak Split Jet (8.6 GtC yr^{-1}; GtC=10^{15} grams-C) is only slightly larger than strong Split Jet (8.4 GtC yr^{-1}). The SAM positive simulation (8.8 GtC yr^{-1}) is somewhat larger than the negative mode (8.3GtC yr^{-1}). If anything, changes in biological production in the weak Split Jet and positive SAM cases should drive more respiration and thus O_2 consumption. The simulated results are opposite (Figure 7).

Interestingly, even while the deep and intermediate waters are clearly more oxygenated in the weak Split Jet and positive SAM runs (Figures 7, 8), the oxygen minimum zone in the eastern equatorial Pacific Ocean is larger in those cases. The volume of water with O_2 concentrations below 2 μmol kg^{-1} is larger in the weak Split Jet case (5.36×10^{15} m^3) than in the strong Split Jet case (5.05×10^{15} m^3). It is also larger in the positive SAM case (5.97×10^{15} m^3) than in the negative SAM case (4.77×10^{15} m^3). While the exact volumes would be overestimated in the OCMIP formulation because denitrification is neglected, as already noted, the sense of change should be correct. It seems puzzling then that the generally better oxygenated oceans (weak Split Jet and positive SAM) have larger tropical Pacific OMZs. However, our results are consistent with the theory that the southward expansion of the South Pacific subtropical gyres prevents northward transport of well-ventilated thermocline waters originating from the subantarctic [*Getzlaff et al.*, 2016].

In summary, both a weaker Split Jet and positive SAM lead to increased ventilation of bottom waters, and with changes associated with positive SAM being larger. The positive SAM also leads to increased ventilation of AAIW waters in all basins, whereas the weaker Split Jet leads to increased ventilation of the SAMW in the South Pacific. In both cases, the oxygen minimum zone region of the eastern equatorial ocean increases.

5.2 Atmospheric pCO_2 and oceanic DIC

Atmospheric pCO_2 is strongly controlled by deep ocean ventilation [*Knox and McElroy*, 1984; *Sarmiento and Toggweiler*, 1984; *Siegenthaler and Wenk*, 1984]. Therefore, the enhanced deep ventilation in the weak Split Jet (vs. strong Split Jet) and positive SAM (vs. negative SAM) simulations would predict an increase in atmospheric pCO_2. The simulated response of atmospheric pCO_2 in the weak Split Jet and positive SAM is indeed positive but unexpectedly small. After 600 years of model integration, the positive pCO_2 anomaly is just over 1 ppm in the weak Split Jet runs and about 3 ppm in the positive SAM runs.

In the Pacific, the zonally averaged the dissolved inorganic carbon (DIC) anomalies for the two cases (Figure 7e,f) have spatial patterns very similar to those of ideal age (Figure 6b,c) and O_2 (Figure 7b,c). The strong negative DIC anomaly in the deep ocean thus indicates that carbon is lost by enhanced ventilation under both the weak-strong Split Jet and positive-negative SAM simulations. Clearly this carbon lost from the deep ocean did not accumulate in the atmosphere, since atmospheric pCO_2 changed only 1-3 ppm.

There are two processes that can put the carbon vented from the deep ocean back into the ocean. The first is the efficient biological utilization of nutrients. This model's diagnostic biological production, based on a 30-day restoring of surface PO_4, ensures that a significant fraction of the nutrients and carbon upwelled in the Southern Ocean are sent back to the ocean interior as organic carbon. To the extent that the restoring is not instantaneous and complete, there will be some leakage of oceanic carbon as both ventilation and export production becomes stronger.

The second process that prevents vented carbon from accumulating in the atmosphere is cooling. The global ocean temperature is cooler by ~0.1 °C in the weak Split Jet case (mean ocean temperature=3.58 °C) compared to the strong Split Jet case (3.67 °C). The cooling in the positive SAM case (3.32 °C) compared to the negative SAM case (3.76 °C) is ~0.44 °C, substantially larger. As gas solubility becomes larger with increased cooling, the weak Split Jet and the positive SAM modes should increase oceanic uptake of carbon relative to their respective opposite modes. In a rough estimate, we calculated the equilibrium DIC concentration with full seawater carbon chemistry for the four cases using ocean mean properties of temperature (noted above), alkalinity (2418 μeq kg^{-1}), salinity (34.73psu), and for equilibrium atmospheric pCO_2 (284.7 ppm). Multiplying the change in mean DIC with the ocean volume and converting the oceanic carbon inventory to ppm, we determine the cooling effect to be ~8 ppm for the weak-strong Split Jet case and ~38 ppm for the positive-negative SAM case. In other words, without the cooling, atmospheric pCO_2 rise should have been much larger, 9 instead of 1 ppm in the Split Jet case, and 41 instead of 3 ppm in the SAM case. This assumes the same degree of air-sea gas equilibration, which is not strictly correct, because the simulated DIC anomaly does not follow the change expected from PO_4 anomaly. If the air-sea CO_2 disequilibrium were constant, DIC should be related to PO_4 by the organic matter C:P stoichiometry of 117, but the trend observed in the model is larger. The simulated C:P ratio in the Southern Pacific is 136 in the Split Jet cases and 190 in the SAM cases. The estimated cooling effect on atmospheric pCO_2 of 8 and 38 ppm should thus be viewed as the upper bound.

Our overall interpretation is that dynamical response of atmospheric pCO_2 to the Split Jet (weak-strong) and SAM (positive-negative) forcing is an increase in the atmospheric CO_2 from increased ventilation of the deep oceans. This result, at least for the SAM response, is qualitatively consistent with many previous studies on the link between ocean carbon and Southern Hemisphere winds (e.g. *d'Orgeville et al.*, 2010; *Lovenduski et al.*, 2007; *Russell et al.*, 2006). The actual change would be much larger than 1-3 ppm, if biological and solubility effects did not dampen the dynamical response. The combination of the deep ocean venting carbon in the Southern Ocean, but the ocean largely maintaining its carbon inventory, results in a redistribution of the DIC anomaly as seen in Figure 7. DIC is effectively stored outside the Southern Ocean and deep ocean, where ventilation remains the same or is slightly less vigorous (Figure 6). This is more clearly evident in the positive-negative SAM simulations (Figure 7f).

6. Comparison to Paleoproxy records during the Early Deglacial Period

To illustrate the applicability of the modeling results to interpreting Southern Hemisphere westerly changes in past climates, we examine paleoceanographic changes during the early deglacial period following the Last Glacial Maximum (LGM), linked to the Heinrich 1 event. The period during Heinrich 1 is particularly interesting for examining changes to the Southern Hemisphere westerlies and Southern Ocean circulation. This period marks the beginning of the last glacial termination when CO_2 started rising and Northern Hemisphere ice sheets started melting (*Denton et al*. 2010). While Heinrich 1 occurred in the North Atlantic with armadas of icebergs entering the ocean there, studies have shown synchronous climate changes in distant Southern Hemisphere locations timed to Heinrich 1, in particular changes in the Southern Hemisphere westerlies and ocean circulation (e.g. *Lamy et al. 2007*, *Anderson et al.*, 2009). Increase to upwelling over the Southern Ocean and resulting flux of carbon from the deep ocean to the atmosphere during Heinrich 1 are thought to provide the initial deglacial rise in CO_2 (*Lamy et la. 2007, Anderson et al. 2009, Denton et al. 2010*).

We focus on specific circulation features as identified by the simulations, and which may distinguish between a Split Jet response or SAM response; as it turns out, paleoproxy records during Heinrich 1 suggest pronounced changes for all the features of interest. We note the limitations to this comparison: while our simulated ocean changes are for the annual mean (and using wintertime atmospheric forcing changes), proxy records can be records of annual means, or of a particular season. This should be kept in mind in reading this section.

6.1 Changes to currents in the East Australian-New Zealand sector

There is paleoproxy evidence for changes to the ocean circulation and climate over the East Australian – New Zealand sector during the early deglaciation consistent with the impacts of a Split Jet weakening. First, *Felis et al.* [2014] showed that SST over the southeastern coral sea (around 22.6°S, 161.7°E) as well as SSTs over the Great Barrier Reef (17.1°S, 146.6°E and, 19.7°S, 150.3°E) warmed during this period. Second, *Schiraldi et al.* [2014] argue, based on proxy records in the Bay of Plenty (north of North Island of New Zealand, around 37°S, 177°E), that the water source changed there from an Antarctic source to a tropical one; and that a proxy farther south in Hawke Bay (MD97-2121 40.38°S, 178°E; *Carter et al.*, 2008) also shows more influence from tropical sources. Both proxies are consistent with the impact of a weaker Split Jet but not with a more positive SAM (Figure 4b, c; the green triangles in those figures show the location of the proxies). In particular, strengthening of the South Pacific subtropical gyre in the weak Split Jet leads to a stronger Tasman front that crosses over to northern New Zealand and feeds into the East Auckland and then the East Cape Current off the eastern coast of North Island; this would explain the increased prevalence of tropically-sourced waters. On the other hand, a positive SAM leads to a *weaker* East Auckland and East Cape current (Figure 4c).

Furthermore, there is robust proxy evidence that argues for a southward shift of the Subtropical Front during the early deglaciation that implicates changes to the Southern Hemisphere westerlies, though both a weaker Split Jet and positive phase of the SAM may produce this change. *Bostock et al.* [2015] show from a transect of cores (see figure 4, green line south of New Zealand, for the location) that the southern Subtropical Front by the Solander

Trough rapidly shifted southwards during the early deglaciation (18-16ka) with respect to its modern position. *Sikes et al.* [2009] show that the Subtropical Front south of Tasmania (figure 4, green line south of Tasmania) also shifted southwards during deglaciation. Warming of SST south of Tasmania and New Zealand indicates a southward shift of the Subtropical Front, which is consistent with the East Australian Current penetrating farther south. This could be the result of either a weaker Split Jet or positive SAM, or both.

6.2 Changes to Drake Passage Throughflow and southeastern Pacific

There is evidence for a substantial increase to the Drake Passage throughflow during the early deglacial period that argues more for a positive-SAM like change. *Lamy et al.* [2015] used grain size distributions in cores along the Drake Passage to argue for a 40% decrease in Drake Passage northernmost flow during glacial times compared to present, coupled with a stronger northward current along Chile. During Heinrich 1, Drake Passage transport – mainly over the Subantarctic region – reinvigorated, though the magnitude was not reported. In our simulations, both a weaker Split Jet and a positive SAM lead to a stronger Drake Passage throughflow, though the change is much stronger with a positive SAM. This observation might argue that a positive SAM was a more likely scenario for the Heinrich 1 period.

We note that sediment proxies along the coast of Southern Chile have shown a strong warming in SST in the southeastern Pacific off the coast of southern Chile timed to Heinrich 1 (in particular site ODP1233 at 41°S, 74.2°W) (*Lamy et al.*, 2007; *Mohtadi et al.*, 2008). Lamy et al. (2015) partly attribute this warming to an increased Drake Passage throughflow, that then lessened the northward advection of subantarctic waters northwards towards southern Chile. We note that our simulations show no evidence of significant warming for a weak Split Jet or positive SAM (figure 4b,c), and in fact for a weaker Split Jet shows a moderate cooling around

41°S in the southeastern Pacific. We speculate that the ocean model may not have sufficient horizontal resolution to resolve key processes that determine SST and its changes at the ODP1233 location. This includes resolving the sharp meridional SST front over that region, as well as coastal upwelling and coastal current processes.

6.3 Changes to Mode/Intermediate Water formation

Proxy evidence generally indicates an increase in either Antarctic Intermediate Water (AAIW) or the Subantarctic Mode Water (SAMW) formation during early deglaciation (figure 9 shows the location of the proxies discussed). *Pahnke and Zahn* [2005] found evidence for increased AAIW formation during H stadials as seen in the record by Chatham Rise to the east of New Zealand; this is corroborated by a record in the middle depths of the Brazil Margin [*Pahnke et al.*, 2008] that showed similar changes during H1 and the Younger Dryas. *Pena et al.* [2013] argue, from an Nd proxy record in the southeastern equatorial Pacific, for a stronger intrusion of southern intermediate waters into the equatorial undercurrent during North Atlantic cold periods, including H1.

Comparison of these records with the ideal age changes in our simulations – with a reduced ideal age interpreted to be increased intermediate water formation - is equivocal. The *Pahnke and Zahn (2005)* record is consistent with both a weak Split Jet or positive SAM change; the simulated ocean ideal age decreases in both instances at the Pahnke and Zahn (2005) site off Chatham rise (figure 9a & b, left panels), though the weak Split Jet response appears to have a stronger influence. However, neither the Split Jet nor the SAM modulations produce the necessary changes seen in the Brazil Margin (figure 9a & b, center panels), though we point out that changes to the Atlantic Meridional Overturning Circulation (AMOC) during H1 – and not represented in our simulations – likely have a larger influence on intermediate waters in this region. There is intriguing evidence that a weaker Split Jet can explain the *Pena et al. (2013)* equatorial undercurrent record. A weaker Split Jet leads to increased rate of SAMW formation over the entire tropical Pacific (cf Fig 8a), and waters at intermediate depths over the equatorial region are younger for a weaker Split Jet (figure 9a, right panel); on the other hand, they are older for a positive SAM (Figure 9b, right panel).

Muratli et al. (2010) inferred *decreasing* AAIW ventilation during the early deglacial warming, based on decreasing oxygen inferred from three ODP cores (1233, 1234, and 1235) along the Chilean coast and intermediate depths record. This observation appears to be contrary to the increased intermediate water formation simulated from the weaker Split Jet or positive SAM phase. However, examination of the simulated dissolved O_2 along 75.5°W (the gridpoint closest to the coastline) actually shows *reduced* oxygen concentration for the weak Split Jet, and to a lesser extent a positive SAM (figure 9c,d), at least for the two equatorward cores (1234 and 1235). The decreased oxygen appears not to be from intermediate waters from the south (which shows *increased* oxygen levels, consistent with the increased ventilation), but rather from the surface undercurrent and Pacific Deep Water originating from the north. We thus suggest that our inference of increased intermediate formation from the weaker Split Jet or positive SAM might not be inconsistent with the *Muratli et al. (2010)* result.

Overall, the evidence from intermediate water formation somewhat favors a weakened Split Jet over the positive SAM during the early deglacial period, as it more readily explains the *Pahnke and Zahn (2005), Pena et al. (2013),* and *Muratli et al. (2010)* observations.

6.4 Changes to the Meridional Overturning Circulation

It is by now well-established that increased ventilation of Antarctic circumpolar deep water occurred during Heinrich 1 (e.g. *Anderson et al.*, 2009; *Skinner et al.*, 2010*; Siani et al., 2013*). Since both a weaker Split Jet and a positive SAM lead to increased ventilation of bottom waters, this observation does not distinguish between the two wind forcings (though the magnitude is stronger in the positive SAM case). *Anderson et al.* [2009] however found increased burial of biogenic opal, interpreted as increased upwelling, at three core locations during H1: 53.2S 5.1E (TN057-13-4PC); 59.62S 155.24E(E27-29); and 61.9S 170W (NBP9802-6PC). If we compare the simulated upwelling changes at these three locations (Figure 5b,c - green triangles), there is no compelling match with either forcing – indeed in two of the three core locations, the change in upwelling is of one sign with the weaker SJ, and of the other in the positive SAM. Hence, the Anderson et al. (2009) proxy record cannot be readily explained by either the weak Split Jet nor positive SAM forcing. Note however that the spatial structure of upwelling changes has relatively small-scale variations, making it difficult to do a convincing model-proxy comparison given the inherent spatial biases in model simulations.

While there is controversy regarding direct ventilation of the North Pacific Ocean in the subarctic during H1 [*Jaccard and Galbraith*, 2013; *Okazaki et al.*, 2010], we are not aware of any paleoproxy evidence in support or against the idea of enhanced deep Pacific oxygenation from the south (Figure 7). Recently published redox sensitive trace metal data indicate increased ventilation and oxygenation of the deep Southern Ocean during northern stadials [*Jaccard et al.*, 2016], but these data are from the Atlantic sector.

7. Conclusion

We investigate ocean circulation and biogeochemical changes resulting from a modulation of the South Pacific Split Jet, the wind changes being previously proposed by the authors as an alternative hypothesis for Southern Hemisphere westerly wind changes in contrast to Southern Annular Mode changes. We apply wind changes – derived from observed Southern Hemisphere wintertime interannual variability – on an ocean general circulation model (POP2) with a simple formulation for ocean biogeochemistry. The most notable features of a weakening of the Split jet is a strengthening and southward displacement of the South Pacific subtropical gyre, that leads to pronounced circulation and temperature changes over the East Australian/New Zealand sector. A weaker Split Jet and a positive SAM result in some similar responses and some distinctly different ones. Similar responses include (i) increased ventilation of bottom waters, though the SAM appears significantly more effective; and (ii) a southward shift of the subpolar front over the New Zealand sector. Distinct responses of a weaker Split Jet include enhanced Subantarctic Mode Water formation in the South Pacific, and a stronger subtropical gyre that leads to a stronger East Australian current that feeds into the Tasman Front and East Auckland/East Cape current; as a result, SSTs are warmer east of northeastern Australia and surrounding New Zealand. Distinct responses to a positive SAM are significantly increased Drake Passage throughflow and ventilation of the Antarctic Intermediate Waters over all basins.

We thus identify key oceanic responses that could uniquely distinguish between the modulation of the Split Jet and a modulation of the SAM. Our limited comparison of existing published paleoceanographic records of the early deglacial period however finds evidence for both a weaker Split Jet and positive SAM: notably, the observed SST warming off the Great Barrier Reef [*Felis et al.*, 2014] and northern New Zealand [*Schiraldi et al.*, 2014] suggests a weaker Split Jet, whereas the increased Drake Passage throughflow [*Lamy et al.*, 2015] favors a positive SAM response. Intermediate water proxies suggest that both a weaker Split Jet and positive SAM are possible, though more consistent with the former.

Note that the wind responses are not exclusive of each other: both can occur at the same time, and in fact this is the interpretation we favor for the early deglacial period based on our comparison. We have done an additional set of ocean simulations using forcing where we added the weak Split Jet and positive SAM winds, and compared against a simulation adding a strong Split Jet with negative SAM conditions; to first order, we find that the results appear to be a linear combination of the two individual forcings, with no significant nonlinearities (figures not shown). We note that in our previous modeling study that proposed an atmospheric teleconnection from North Atlantic cooling to the southern hemisphere westerlies via a southward ITCZ shift [*Lee et al.*, 2011], the southern hemisphere westerly response resembled a mixture of a weaker Split Jet and positive SAM (see figure 5a of Lee et al. 2011).

The modulation of the Split Jet appears to be extremely effective at changing the temperature climate over the New Zealand sector. *Chiang et al. (2014)* previously noted that a weaker Split Jet is effective at warming New Zealand by allowing tropical airmasses to penetrate further southwards. This study shows that the ocean response to a weaker Split Jet also warms the ocean temperatures surrounding New Zealand (figure 4b). Previous work had documented pronounced and rapid reduction to glacier length there during Heinrich 1 (Putnam et al., 2013) and Younger Dryas (Kaplan et al. 2010), and the opposite during the Antarctic cold reversal (Putnam et al. 2010). We advance the Split Jet modulation as a plausible mechanism for explaining the rapid climate changes occurring over New Zealand during deglaciation.

There have been many previous studies on the ocean response to changing southern hemisphere westerlies. A distinct advantage of our study over most other such studies is that, by deriving wind changes from observed interannual variability, we are using wind forcings that are physically realizable, albeit large. The realism of our forcing and model setup allows us to make specific regional predictions that can be contrasted against paleoproxy data.

There are clear limitations to our study. First, we are using simulations embedded within a modern-day basic state, so the assumption is that the glacial basic state ocean circulation is qualitatively similar. Second, our winds are applied only to the austral winter, so we omit the influence of changes to the austral summer (though we could undertake a similar study for that season). Third, the winds we apply are steady in time, and we do not allow changes to high-frequency weather disturbances; in reality, the position of storm tracks will change as the mean flow changes. Finally, we are using an ocean model that does not permit ocean eddies, which are demonstrated to be important to understanding Southern Ocean circulation and in particular the effect on the strength of the ACC and the Southern Ocean meridional overturning circulation [*Gent*, 2016]; we are in effect relying on the model's parameterizations to provide estimates of the influence of eddies on the ocean general circulation. However, we note that the ocean model we use employs a variable coefficient in the Gent-McWilliams eddy parameterization, and *Gent and Danabasoglu* [2011] showed that the response of this model to increased Southern Hemisphere westerlies appear realistic as compared to eddy-permitting models.

Finally, we know that the early deglacial period was marked by a slowdown of the AMOC, and there is a global ocean adjustment to this slowdown that is separate and distinct from the changes in response to the southern hemisphere wind changes. It may well be that such adjustments could also explain some of the paleoproxy changes discussed in section 6. Contrasting the direct effect of AMOC changes on Southern Ocean circulation with those of the southern hemisphere westerly changes will be the focus of a future study.

Acknowledgments, Samples, and Data

The CESM forcing files and model output used is available for download at https://doi.org/10.6078/D1PM3T (*Chiang et al. 2017*). This work was funded by NSF grant 1537496 to JCHC, and NSF grant 1537105 to KM. The Community Earth System Model was developed by the National Center for Atmospheric Research (NCAR). We thank Keith Lindsay at NCAR for providing the ocean biogeochemistry module used in our model simulations. We acknowledge high-performance computing support for the CESM simulations from the Yellowstone cluster (ark:/85065/d7wd3xhc) provided by NCAR's Computational and Information Systems Laboratory, sponsored by the National Science Foundation. The CORE v2 data are obtained from a website hosted by the Geophysical Fluid Dynamics Laboratory: http://data1.gfdl.noaa.gov/nomads/forms/core/COREv2.html. The Southern Annular Mode index used to compare against the wind EOF2 timeseries in section 3 was obtained from the NOAA CPC website: http://www.cpc.ncep.noaa.gov/products/precip/CWlink/daily_ao_index/aao/aao.shtml.

References

Anderson, R. F., S. Ali, L. I. Bradtmiller, S. H. H. Nielsen, M. Q. Fleisher, B. E. Anderson, and L. H. Burckle (2009), Wind-Driven Upwelling in the Southern Ocean and the Deglacial Rise in Atmospheric CO2, *Science*, *323*(5920), 1443-1448, doi:Doi 10.1126/Science.1167441.

Bals-Elsholz, T. M., E. H. Atallah, L. F. Bosart, T. A. Wasula, M. J. Cempa, and A. R. Lupo (2001), The wintertime Southern Hemisphere split jet: Structure, variability, and evolution, *Journal of Climate*, *14*(21), 4191-4215.

Bostock, H. C., B. W. Hayward, H. L. Neil, A. T. Sabaa, and G. H. Scott (2015), Changes in the position of the Subtropical Front south of New Zealand since the last glacial period, *Paleoceanography*, *30*(7), 824-844.

Cai, W., G. Shi, T. Cowan, D. Bi, and J. Ribbe (2005), The response of the Southern Annular Mode, the East Australian Current, and the southern mid-latitude ocean circulation to global warming, *Geophysical Research Letters*, *32*(23).

Carter, L., B. Manighetti, G. Ganssen, and L. Northcote (2008), Southwest Pacific modulation of abrupt climate change during the Antarctic Cold Reversal–Younger Dryas, *Palaeogeography, Palaeoclimatology, Palaeoecology*, *260*(1), 284-298.

Chiang, J. C. H., and A. R. Friedman (2012), Extratropical Cooling, Interhemispheric Thermal Gradients, and Tropical Climate Change, *Annual Review of Earth and Planetary Sciences*, *40*(1), 383-412, doi:10.1146/annurev-earth-042711-105545.

Chiang, J. C. H., S.-Y. Lee, A. E. Putnam, and X. Wang (2014), South Pacific Split Jet, ITCZ shifts, and atmospheric North–South linkages during abrupt climate changes of the last glacial period, *Earth and Planetary Science Letters*, *406*(0), 233-246, doi:http://dx.doi.org/10.1016/j.epsl.2014.09.012.

Chiang, J. C. H., K. Tokos, S.-Y. Lee, and K. Matsumoto (2017), Forcing files and Model output for "Contrasting impacts of the South Pacific Split Jet and the Southern Annular Mode modulation on Southern Ocean circulation and biogeochemistry", v2, UC Berkeley Dash, Dataset, https://doi.org/10.6078/D1PM3T

d'Orgeville, M., nbsp, W. Sijp, M. England, and K. Meissner (2010), On the control of glacial-interglacial atmospheric CO2 variations by the Southern Hemisphere westerlies, *Geophysical Research Letters*, *37*(21).

Danabasoglu, G., S. C. Bates, B. P. Briegleb, S. R. Jayne, M. Jochum, W. G. Large, S. Peacock, and S. G. Yeager (2011), The CCSM4 Ocean Component, *Journal of Climate*, *25*(5), 1361-1389, doi:10.1175/JCLI-D-11-00091.1.

Denton, G. H., Anderson, R. F., Toggweiler, J. R., Edwards, R. L., Schaefer, J. M., & Putnam, A. E. (2010). The last glacial termination. *Science*, *328*(5986), 1652-1656.

Felis, T., H. V. McGregor, B. K. Linsley, A. W. Tudhope, M. K. Gagan, A. Suzuki, M. Inoue, A. L. Thomas, T. M. Esat, and W. G. Thompson (2014), Intensification of the meridional temperature gradient in the Great Barrier Reef following the Last Glacial Maximum, *Nature communications*, *5*.

Fletcher, M. S., and P. I. Moreno (2011), Zonally symmetric changes in the strength and position of the Southern Westerlies drove atmospheric CO2 variations over the past 14 k.y., *Geology*, *39*(5), 419-422, doi:Doi 10.1130/G31807.1.

Gent, P. R. (2016), Effects of Southern Hemisphere wind changes on the meridional overturning circulation in ocean models, *Annual review of marine science*, *8*, 79-94.

Gent, P. R., and G. Danabasoglu (2011), Response to increasing Southern Hemisphere winds in CCSM4, *Journal of climate*, *24*(19), 4992-4998.

Getzlaff, J., H. Dietze, and A. Oschlies (2016), Simulated effects of southern hemispheric wind changes on the Pacific oxygen minimum zone, *Geophysical Research Letters*, *43*(2), 728-734.

Inatsu, M., and B. J. Hoskins (2004), The zonal asymmetry of the Southern Hemisphere winter storm track, *Journal of Climate*, *17*(24), 4882-4892.

Jaccard, S., and E. Galbraith (2013), Direct ventilation of the North Pacific did not reach the deep ocean during the last deglaciation, *Geophysical Research Letters*, *40*(1), 199-203.

Jaccard, S. L., E. D. Galbraith, A. Martinez-Garcia, and R. F. Anderson (2016), Covariation of deep Southern Ocean oxygenation and atmospheric CO^ sub 2^ through the last ice age, *Nature*, *530*(7589), 207.

Kaplan, Michael R., Joerg M. Schaefer, George H. Denton, David JA Barrell, Trevor JH Chinn, Aaron E. Putnam, Bjørn G. Andersen, Robert C. Finkel, Roseanne Schwartz, and Alice M. Doughty. "Glacier retreat in New Zealand during the Younger Dryas stadial." *Nature* 467, no. 7312 (2010): 194-197.

Knox, F., and M. B. McElroy (1984), Changes in atmospheric CO2: Influence of the marine biota at high latitude, *Journal of Geophysical Research: Atmospheres*, *89*(D3), 4629-4637.

Lamy, F., H. W. Arz, R. Kilian, C. B. Lange, L. Lembke-Jene, M. Wengler, J. Kaiser, O. Baeza-Urrea, I. R. Hall, and N. Harada (2015), Glacial reduction and millennial-scale variations in Drake Passage throughflow, *Proceedings of the National Academy of Sciences*, *112*(44), 13496-13501.

Lamy, F., J. Kaiser, H. W. Arz, D. Hebbeln, U. Ninnemann, O. Timm, A. Timmermann, and J. R. Toggweiler (2007), Modulation of the bipolar seesaw in the southeast pacific during Termination 1, *Earth and Planetary Science Letters*, *259*(3-4), 400-413, doi:Doi 10.1016/J.Epsl.2007.04.040.

Large, W., and S. Yeager (2009), The global climatology of an interannually varying air–sea flux data set, *Climate Dynamics*, *33*(2-3), 341-364.

Lee, S. Y., J. C. H. Chiang, K. Matsumoto, and K. S. Tokos (2011), Southern Ocean wind response to North Atlantic cooling and the rise in atmospheric CO(2): Modeling perspective and paleoceanographic implications, *Paleoceanography*, *26*, doi:Artn Pa1214 Doi 10.1029/2010pa002004.

Lovenduski, N. S., N. Gruber, S. C. Doney, and I. D. Lima (2007), Enhanced CO2 outgassing in the Southern Ocean from a positive phase of the Southern Annular Mode, *Global Biogeochem Cy*, *21*(2).

Marshall, G. J. (2003), Trends in the Southern Annular Mode from observations and reanalyses, *Journal of Climate*, *16*(24), 4134-4143.

Mo, K. C. (2000), Relationships between low-frequency variability in the Southern Hemisphere and sea surface temperature anomalies, *Journal of Climate*, *13*(20), 3599-3610.

Mohtadi, M., P. Rossel, C. B. Lange, S. Pantoja, P. Böning, D. J. Repeta, M. Grunwald, F. Lamy, D. Hebbeln, and H.-J. Brumsack (2008), Deglacial pattern of circulation and marine productivity in the upwelling region off central-south Chile, *Earth and Planetary Science Letters*, *272*(1), 221-230.

Moreno, P. I., J. P. Francois, C. M. Moy, and R. Villa-Martinez (2010), Covariability of the Southern Westerlies and atmospheric CO2 during the Holocene, *Geology*, *38*(8), 727-730, doi:Doi 10.1130/G30962.1.

Muratli, J. M., Chase, Z., Mix, A. C., & McManus, J. (2010). Increased glacial-age ventilation of the Chilean margin by Antarctic Intermediate Water. *Nature Geoscience*, *3*(1), 23-26.

Najjar, R. G., X. Jin, F. Louanchi, O. Aumont, K. Caldeira, S. C. Doney, J. C. Dutay, M. Follows, N. Gruber, and F. Joos (2007), Impact of circulation on export production, dissolved organic matter, and dissolved oxygen in the ocean: Results from Phase II of the Ocean Carbon-cycle Model Intercomparison Project (OCMIP-2), *Global Biogeochem Cy*, *21*(3).

Nakamura, H., and A. Shimpo (2004), Seasonal variations in the Southern Hemisphere storm tracks and jet streams as revealed in a reanalysis dataset, *Journal of Climate*, *17*(9), 1828-1844.

North, G. R., T. L. Bell, R. F. Cahalan, and F. J. Moeng (1982), Sampling errors in the estimation of empirical orthogonal functions, *MWR*, *110*, 699-706.

Okazaki, Y., A. Timmermann, L. Menviel, N. Harada, A. Abe-Ouchi, M. O. Chikamoto, A. Mouchet, and H. Asahi (2010), Deepwater Formation in the North Pacific During the Last Glacial Termination, *Science*, *329*(5988), 200-204, doi:Doi 10.1126/Science.1190612.

Pahnke, K., S. L. Goldstein, and S. R. Hemming (2008), Abrupt changes in Antarctic Intermediate Water circulation over the past 25,000 years, *Nature Geoscience*, *1*(12), 870-874.

Pahnke, K., and R. Zahn (2005), Southern Hemisphere water mass conversion linked with North Atlantic climate variability, *Science*, *307*(5716), 1741-1746.

Pena, L., S. L. Goldstein, S. R. Hemming, K. M. Jones, E. Calvo, C. Pelejero, and I. Cacho (2013), Rapid changes in meridional advection of Southern Ocean intermediate waters to the tropical Pacific during the last 30kyr, *Earth and Planetary Science Letters*, *368*, 20-32.

Preisendorfer, R. W. (1988), *Principal Component Analysis in Meteorology*, 425 pp., Elsevier, Amsterdam.

Putnam, Aaron E., George H. Denton, Joerg M. Schaefer, David JA Barrell, Bjørn G. Andersen, Robert C. Finkel, Roseanne Schwartz, Alice M. Doughty, Michael R. Kaplan, and Christian Schlüchter. "Glacier advance in southern middle-latitudes during the Antarctic Cold Reversal." *Nature Geoscience* 3, no. 10 (2010): 700-704.

Putnam, Aaron E., Joerg M. Schaefer, George H. Denton, David JA Barrell, Bjørn G. Andersen, Tobias NB Koffman, Ann V. Rowan et al. "Warming and glacier recession in the Rakaia valley, Southern Alps of New Zealand, during Heinrich Stadial 1." *Earth and Planetary Science Letters* 382 (2013): 98-110.

Russell, J. L., K. W. Dixon, A. Gnanadesikan, R. J. Stouffer, and J. Toggweiler (2006), The Southern Hemisphere westerlies in a warming world: Propping open the door to the deep ocean, *Journal of Climate*, *19*(24), 6382-6390.

Sarmiento, J., and J. Toggweiler (1984), A new model for the role of the oceans in determining atmospheric pCO 2, *Nature*, *308*(5960), 621-624.

Schiraldi, B., E. L. Sikes, A. C. Elmore, M. S. Cook, and K. A. Rose (2014), Southwest Pacific subtropics responded to last deglacial warming with changes in shallow water sources, *Paleoceanography*, *29*(6), 595-611.

Siani, G., E. Michel, R. De Pol-Holz, T. DeVries, F. Lamy, M. Carel, G. Isguder, F. Dewilde, and A. Lourantou (2013), Carbon isotope records reveal precise timing of enhanced Southern Ocean upwelling during the last deglaciation, *Nature Communications*, *4*.

Siegenthaler, U., and T. Wenk (1984), Rapid atmospheric CO2 variations and ocean circulation, *Nature*, *308*(5960), 624-626.

Sikes, E., W. Howard, C. Samson, T. Mahan, L. Robertson, and J. Volkman (2009), Southern Ocean seasonal temperature and Subtropical Front movement on the South Tasman Rise in the late Quaternary, *Paleoceanography*, *24*(2).

Skinner, L., S. Fallon, C. Waelbroeck, E. Michel, and S. Barker (2010), Ventilation of the deep Southern Ocean and deglacial CO2 rise, *Science*, *328*(5982), 1147-1151.

Taljaard, J. (1972), Synoptic meteorology of the Southern Hemisphere, in *Meteorology of the Southern Hemisphere*, edited, pp. 139-213, Springer.

Thompson, D. W. J., and J. M. Wallace (2000), Annular modes in the extratropical circulation. Part I: Month-to-month variability, *Journal of Climate*, *13*(5), 1000-1016.

Toggweiler, J. R. (2009), Shifting Westerlies, *Science*, *323*(5920), 1434-1435, doi:10.1126/science.1169823.

Toggweiler, J. R., and B. Samuels (1998), On the ocean's large-scale circulation near the limit of no vertical mixing, *Journal of Physical Oceanography*, *28*(9), 1832-1852.

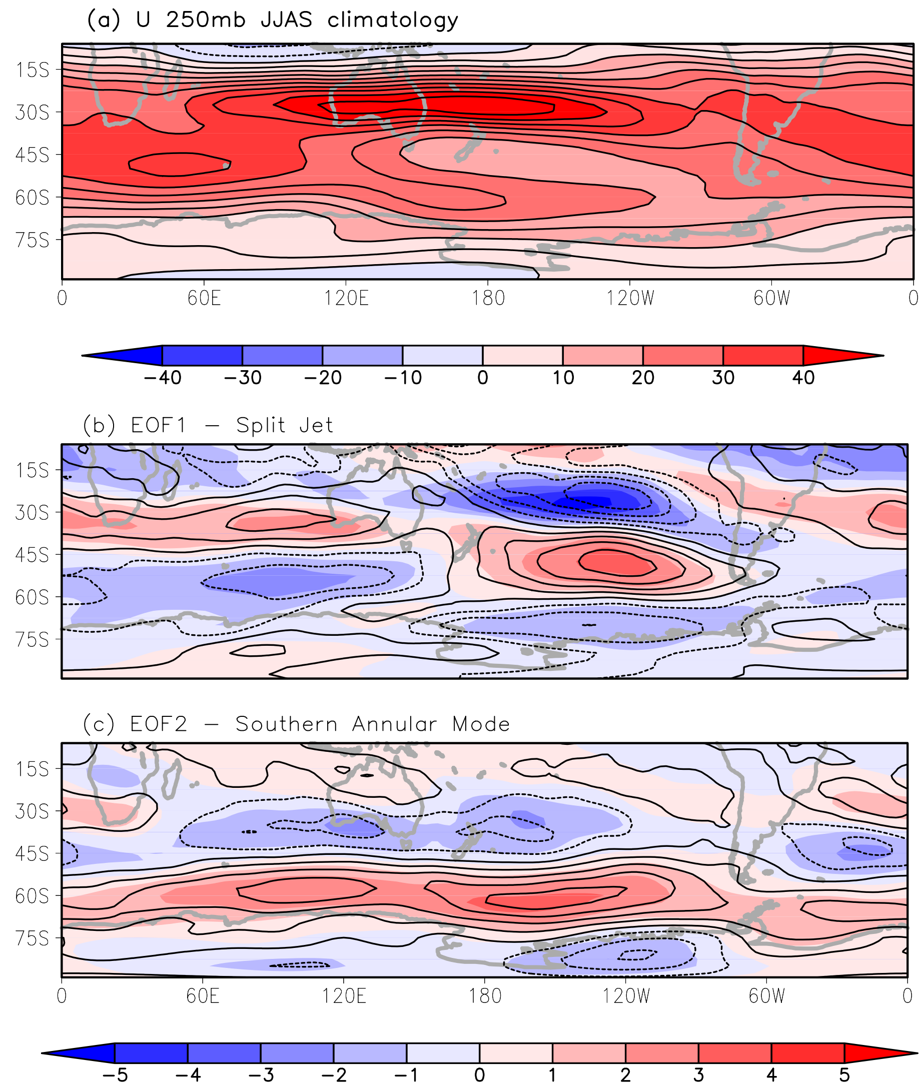

Figure 1. (a) June–September (JJA) 250 mb zonal wind climatology averaged over 1979–2009, showing the presence of the Split Jet in the South Pacific. Contour interval is 5 m/s. (b and c) Mode 1 and mode 2 (respectively) of the 3-D EOF of June-September mean zonal winds from 100-1000mb and 15°S-80°S. The spatial patterns are shown as regression of the normalized principal component onto the June-Sep 250mb zonal winds (shaded) and June-Sep 700mb zonal winds (contours). Units are m/s, and contour interval is 0.5m/s

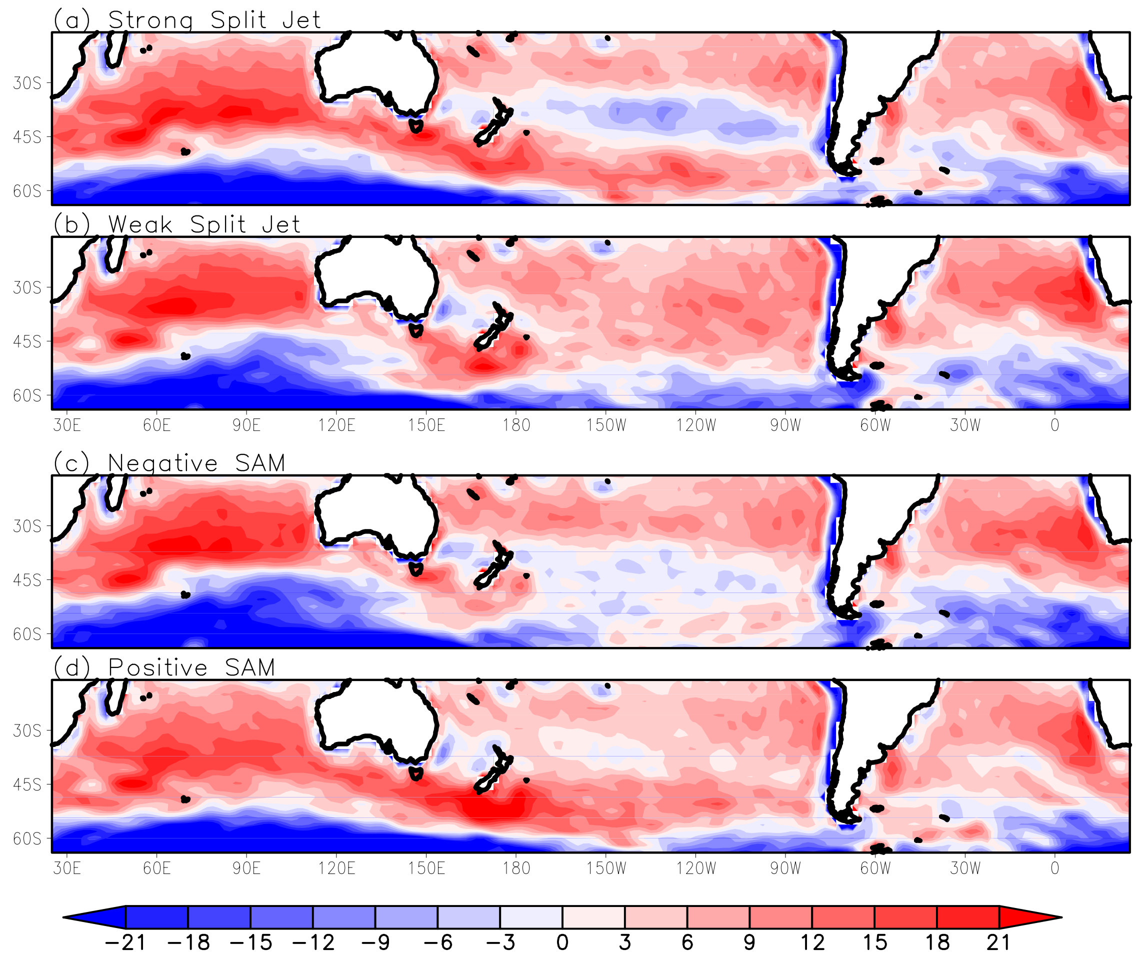

Figure 2. June-September averaged wind stress curl imposed on the ocean model for (a) Strong Split Jet, (b) Weak Split Jet, (c) Negative SAM, and (d) Positive SAM. The fields correspond to a 2σ change to the interannual variation associated with each EOF mode, in both the positive and negative directions (i.e. they are sizable variations, but not unrealistically so). Units are x10^{-8} Pa/m

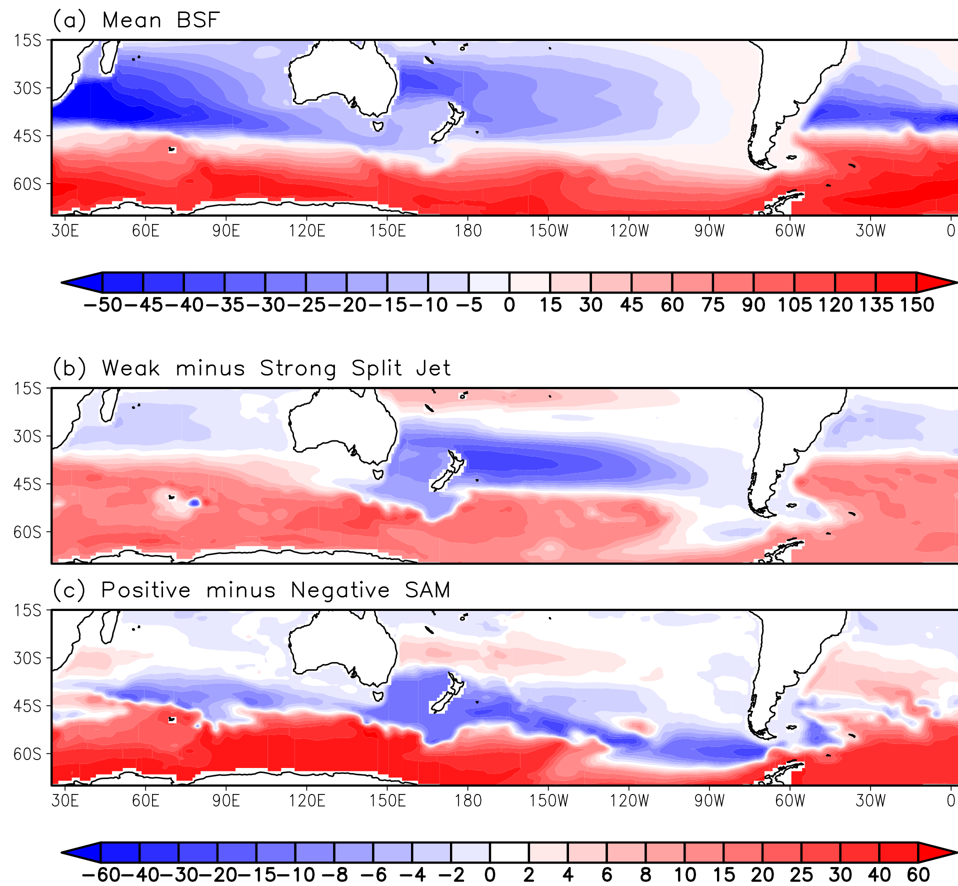

Figure 3. Barotropic streamfunction in the model simulation. (a) Annual mean streamfunction (negative values imply counterclockwise flow). (b) Difference between the weak and strong Split Jet cases. (c) Difference between the positive and negative SAM cases. Units are in Sv. Note the nonlinear scale – in particular for (a), positive intervals are 3x larger than negative intervals.

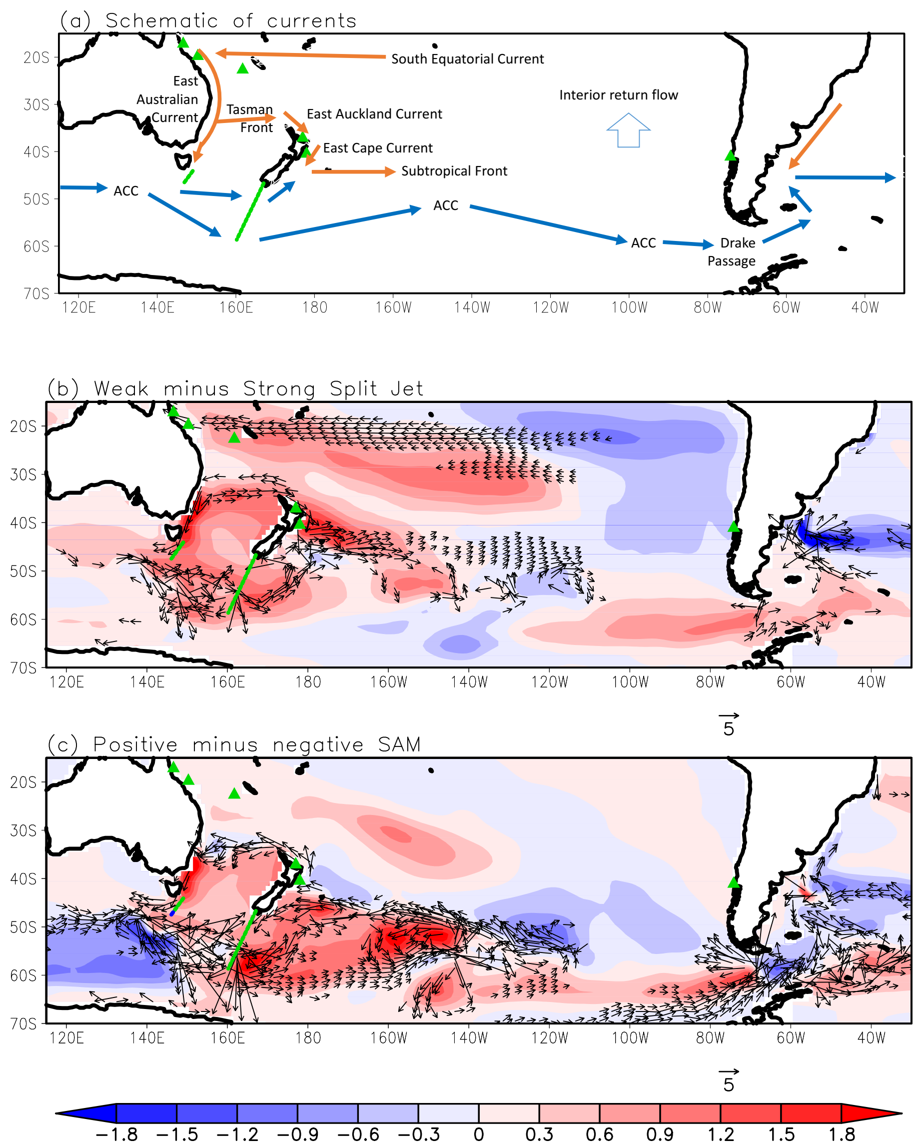

Figure 4. **(a)** Schematic of ocean currents and geographic features discussed in the text. Warm currents are represented in orange, and cold currents in blue. We only include those features highlighted in our analyses. ACC = Antarctic Circumpolar Current. **(b and c)** Sea surface temperature anomaly (color) and surface current anomalies (vectors) for (b) Weak minus Strong Split Jet; and (c) Positive minus Negative SAM. Temperature is in K, and the reference vector is 5 cm/s. Current anomalies below 2 cm/s are not shown. Anomalies are averaged over the upper 100m. Green triangles denote locations of sediment core records for the following (from north to south): Great Barrier reef SST records at 17.1°S, 146.6°E and 19.7°S,150.3°E (Felis et al. 2014); Southeastern coral sea 22.6°S, 161.7°E; Bay of Plenty 37°S, 177°E (Schiraldi Jr et al. 2014); Hawke Bay 40.38°S, 178°E (Carter et al. 2008); and ODP-1233 41°S, 74.2°W (Lamy et al. 2007). The green lines denote the approximate locations of the surface ocean transect investigated in Bostok et al. (2015) south of New Zealand, and in Sikes et al. (2009) south of Tasmania.

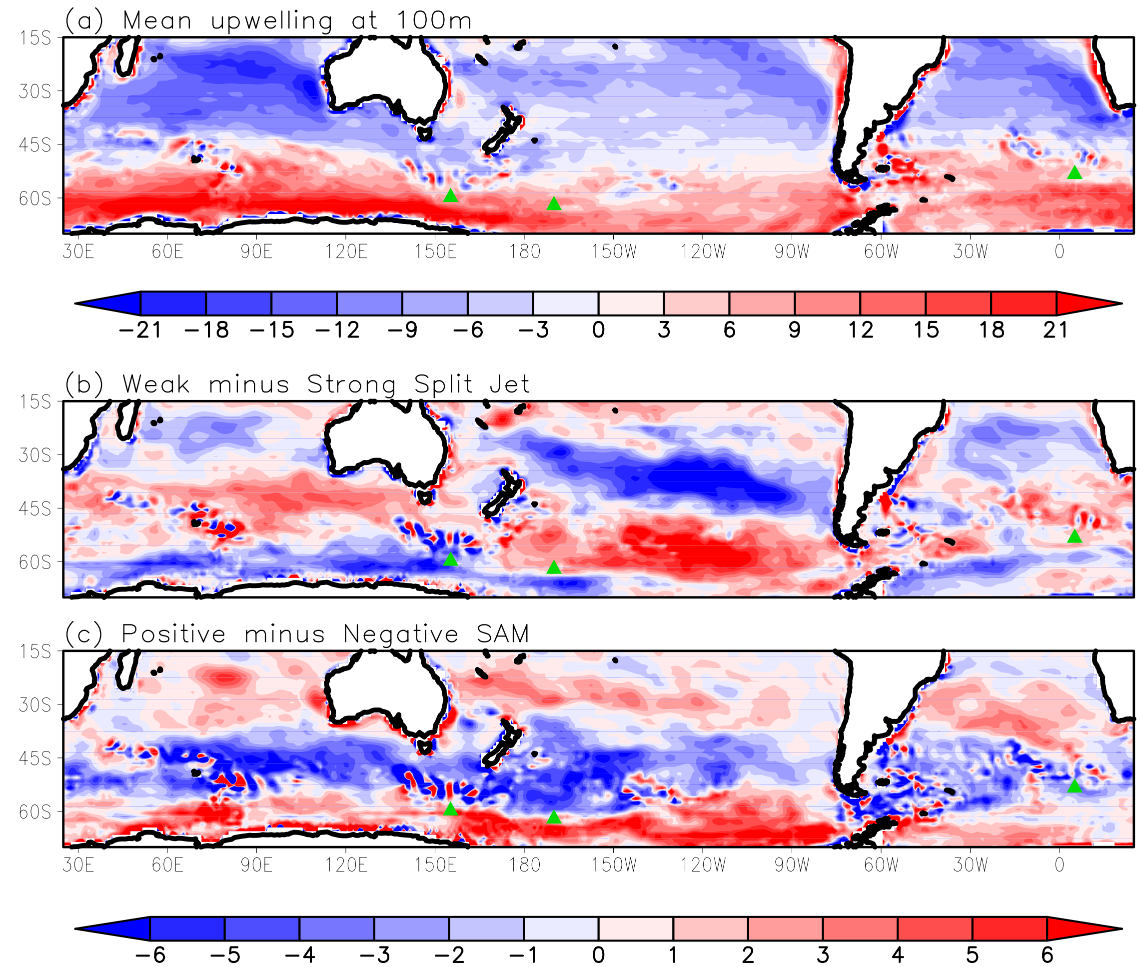

Figure 5. Upwelling at 100m (negative values are downwelling). (a) Annual mean upwelling; (b) Weak minus Strong Split Jet; and (c) Positive minus negative SAM. Units are x10^5 cm/s. Green triangles are the locations to the three core locations (left to right - E27-23: 59.62°S 155.24°E; NBP9802-6PC: 61.9°S 170°W; and TN057-13PC: 53.2°S 5.1°E) in Anderson et al. (2009).

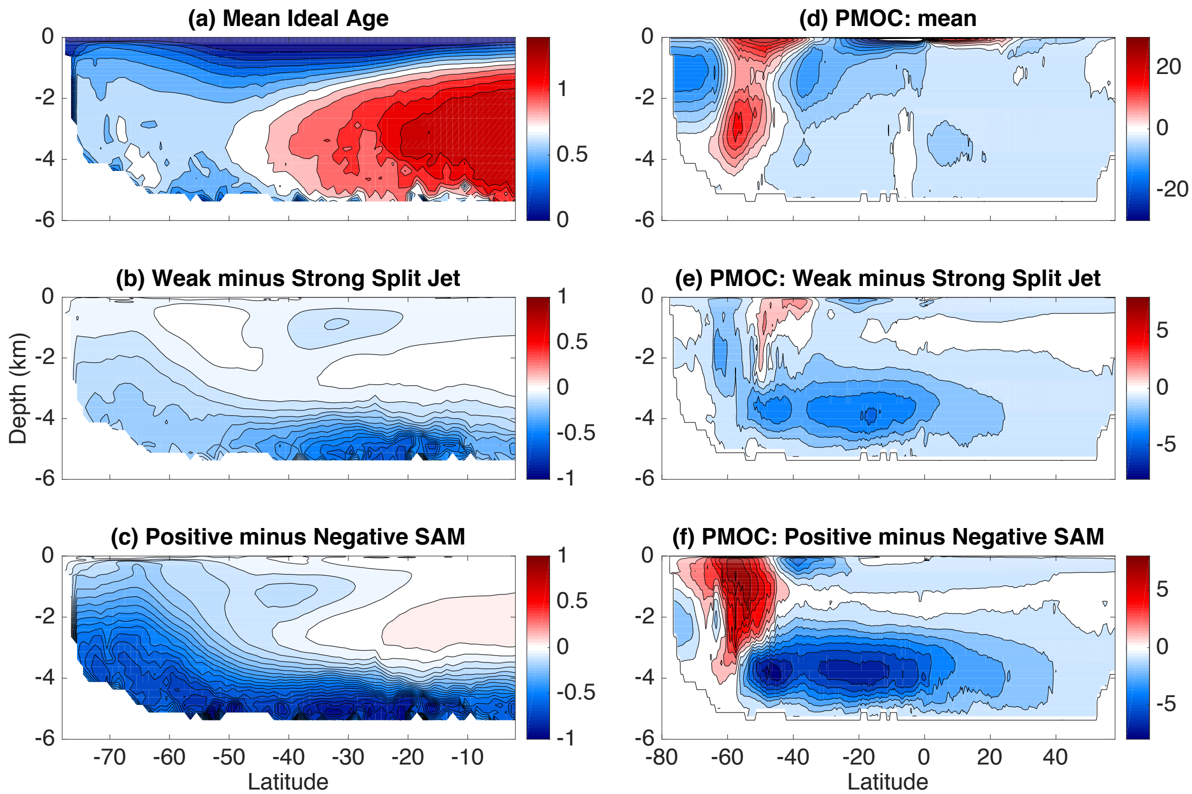

Figure 6. (a-c) Change to the ideal age zonally averaged over the South Pacific Sector (150°E-280°E). The ideal age is the amount of time elapsed since a water parcel left the surface. (a) Mean Ideal Age; (b) Weak minus Strong Split Jet; and (c) Positive minus Negative SAM. Units are kiloyears. Figure shows reduced ideal ages in the ocean interior for both cases indicating increased ventilation, but more pronounced for the SAM case. For a weak Split Jet, ideal age suggests increased ventilation of Subantarctic Mode Water (~30°S and 800m) and Antarctic Bottom Water. For a positive SAM, ideal age suggests increased ventilation of Antarctic Intermediate Water (~40°S and 1200m) and Antarctic Bottom Water. ***(d-f)*** Pacific MOC and its change. (d) Mean circulation; (e) Weak minus Strong Split Jet; and (f) Positive minus Negative SAM. Units are Sv (10^6 m^3 s^{-1}) and the contour interval is 1Sv. Positive values represent clockwise circulation.

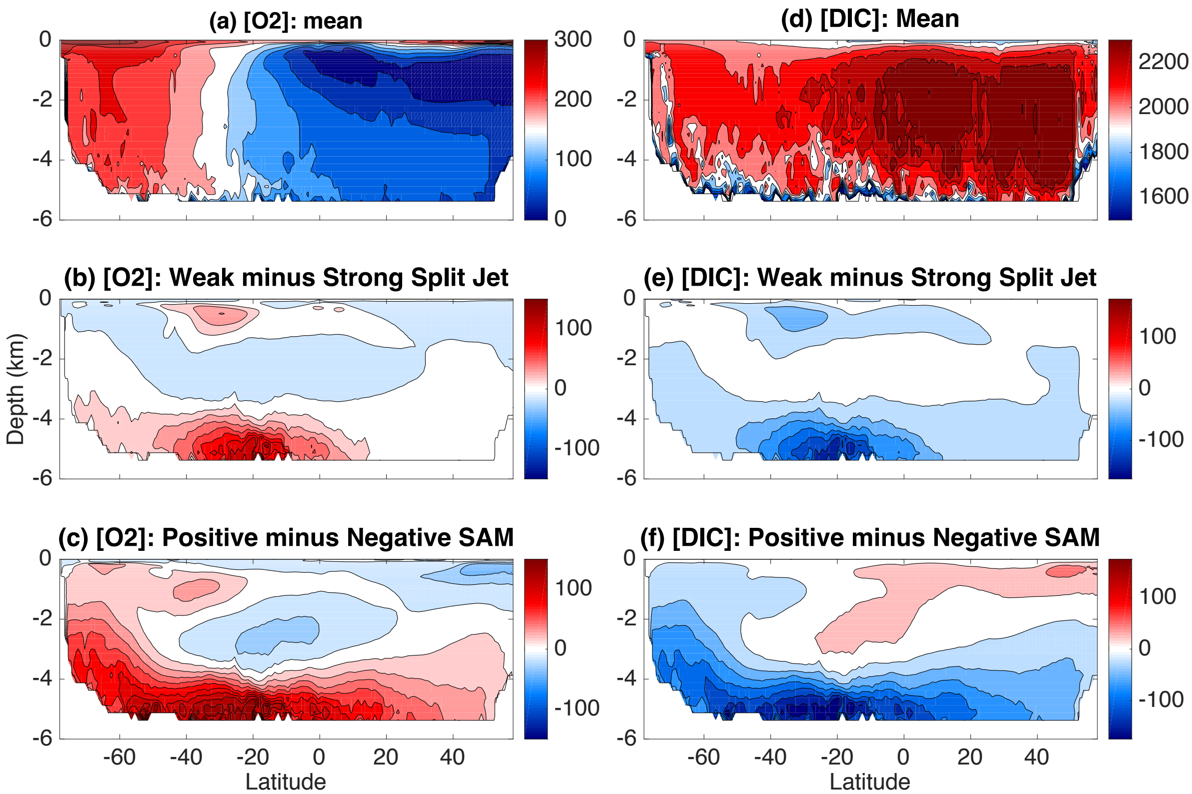

Figure 7. (a-c) Mean field and change in the zonally averaged (150°E-280°E) Pacific dissolved oxygen concentration. (a) Mean (contour interval 30 μmol/kg); (b) Weak minus Strong Split Jet (contour interval 15 μmol/kg); and (c) Positive minus Negative SAM (contour interval 15 μmol/kg). ***(d-f).*** Mean and change in Pacific dissolved inorganic carbon averaged over 150°E-280°E. (d) Mean (contour interval 100 μmol/kg) ; (e) Weak minus Strong Split Jet (contour interval 25 μmol/kg); and (f) Positive minus Negative SAM (contour interval 25 μmol/kg).

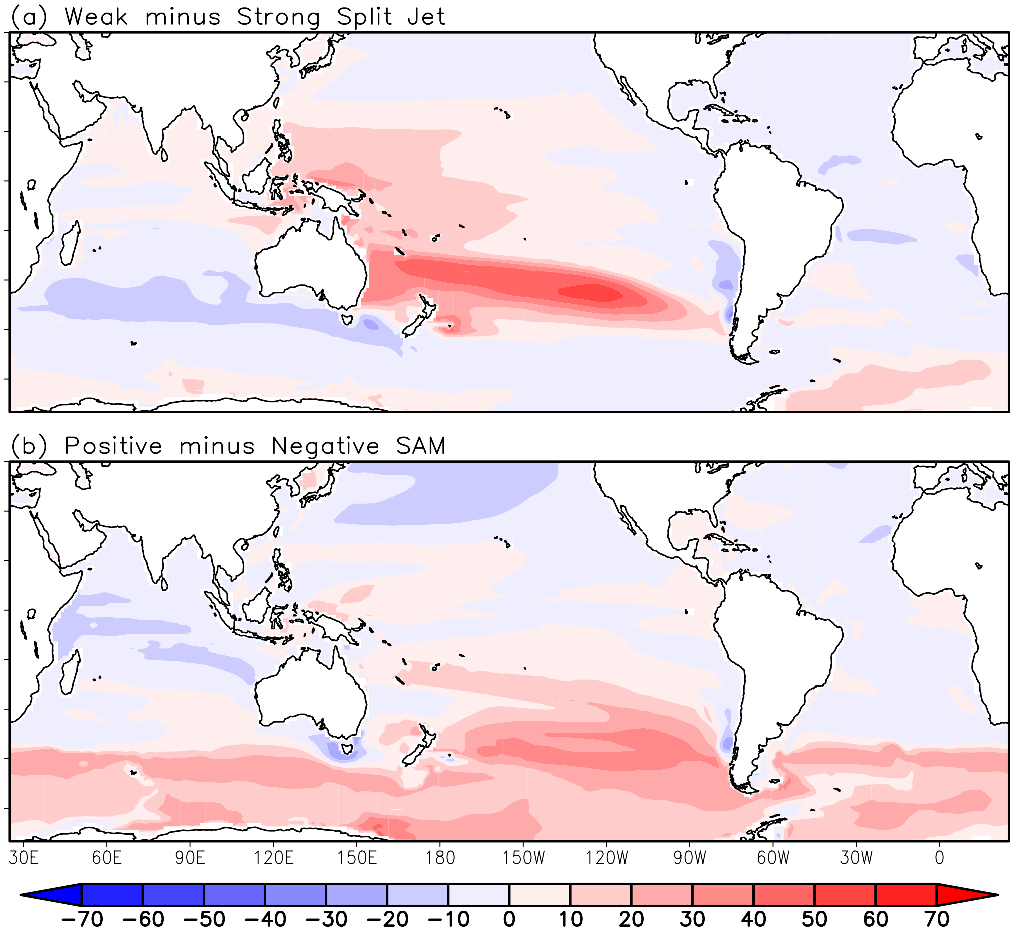

Figure 8. Change to the dissolved O_2 averaged over the upper 1000 m (a) Weak minus Strong Split Jet; and (b) Positive minus Negative SAM. Units are μmol/kg.

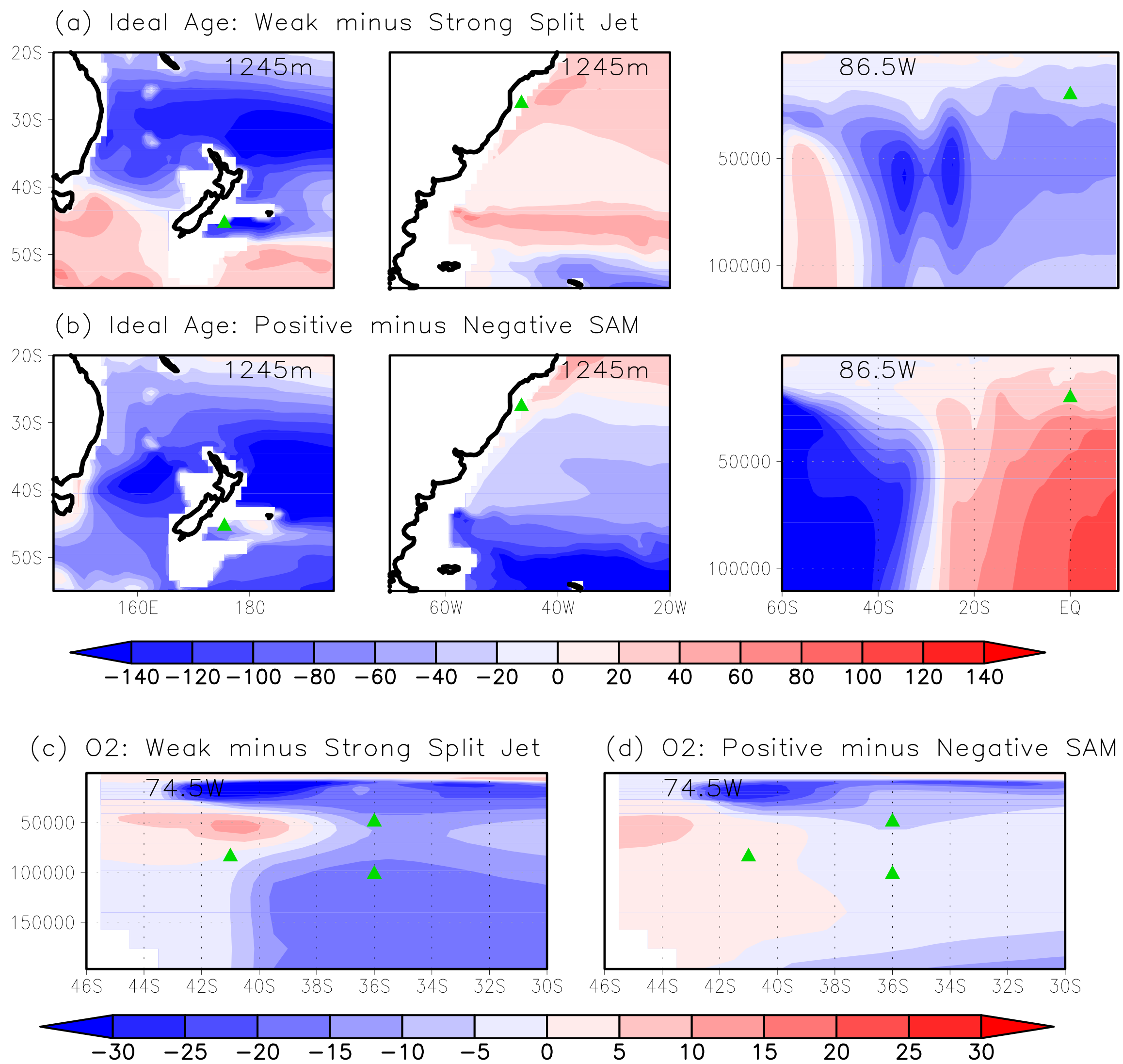

Figure 9. ***(a-b)*** Simulated difference in the ideal age of ocean water over the New Zealand sector (left panels), western south Atlantic (middle panels), and at the southeastern Pacific cross-section at 86.5°W. (a) Weak minus Strong Split Jet. (b) Positive minus Negative SAM. Units are years, and we interpret negative values to mean younger waters and hence more ventilation. For the New Zealand and western south Atlantic sectors, the depth of the water is as indicated in the figure, chosen as the level closest to the proxy record that it is being compared to. For the cross-section, the y-axis depth is in cm. Location of proxy records are as shown in the green triangles (MD27-2120 45.3°S, 175.5°E off New Zealand [Pahnke and Zahn 2005]; KNR159-5-36GGC 27.5°S, 46.5°W off the Brazil Margin [Pahnke et al. 2008]; and ODP 1240 0°N 86.3°W [Pena et al. 2013]). ***(c,d)*** Cross section of dissolved O_2 difference at 74.5°W off the coast of Chile; (c) is for weak minus strong Split Jet, and (d) is for positive minus negative SAM. Units are μmol/kg. The green triangles indicate the positions of ODP cores 1233 (41 °S, 74 W, 838 m), 1234 (36 °S, 73 °W, 1,015 m), and 1235(36 °S, 73 °W, 489 m) reported in *Muratli et al. (2010)*. Y-axis units of depth are in cm.